

Skeletonized Wave-Equation of Surface Wave Dispersion Inversion

Jing Li* and Gerard Schuster, King Abdullah University of Science and Technology

SUMMARY

We present the theory for wave equation inversion of dispersion curves, where the misfit function is the sum of the squared differences between the wavenumbers along the predicted and observed dispersion curves. Similar to wave-equation travel-time inversion, the complicated surface-wave arrivals in traces are skeletonized as simpler data, namely the picked dispersion curves in the (k_x, ω) domain. Solutions to the elastic wave equation and an iterative optimization method are then used to invert these curves for 2D or 3D velocity models. This procedure, denoted as wave equation dispersion inversion (WD), does not require the assumption of a layered model and is less prone to the cycle skipping problems of full waveform inversion (FWI). The synthetic and field data examples demonstrate that WD can accurately reconstruct the S-wave velocity distribution in laterally heterogeneous media.

INTRODUCTION

Inverting surface waves for the S-wave velocity model fall into two categories: 1) the classical method of inverting dispersion curves (Evison et al., 1959; Park et al., 1998; Xia et al., 2004) for a 1D layered medium, and 2) waveform inversion (Groos et al., 2014; Solano et al., 2014; Dou and Ajo-Franklin, 2014) for 2D and 3D media. The classical method accurately inverts for a 1D S-wave velocity model, but becomes less accurate with increasing lateral heterogeneity in the subsurface velocity model. The 1D assumption is not satisfied for some practical applications, so partial remedies are spatial interpolation of 1D velocity models (Tian et al., 2003) and laterally constrained inversion (Socco et al., 2014; Bergamo et al., 2012).

In comparison, full waveform inversion (FWI) can theoretically account for any lateral heterogeneity, but it is computationally expensive and can easily get stuck in local minima associated with the objective function (Tarantola, 1984). To avoid getting stuck in a local minimum, the initial model should be smooth and time-damping strategies can be used at the early iterations (Brossier et al., 2008; Romdhane et al., 2011; Sheng et al., 2006; Sears et al., 2008). However, there are no proven strategies for avoiding local minima in the context of FWI with surface waves.

A partial surface wave FWI method is that of Pérez Solano et al. who used the magnitude spectra of surface waves as the input data (Solano et al., 2014). Results with synthetic data showed this to be a robust and efficient method for reconstructing the S-velocity model at the near surface. Another surface-wave inversion strategy is proposed by (Yuan et al., 2015), who developed a wavelet multi-scale adjoint method which combined surface waves and body waves. Synthetic tests showed that this approach can avoid cycle skipping for some models. The role of attenuation in FWI with surface waves was studied

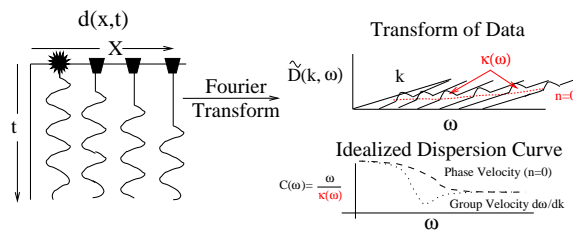


Figure 1: Common shot gather $d(x, t)$ on the left and the fundamental ($n=0$) dispersion curves for Rayleigh waves in the (top right) $k - \omega$ and (bottom right) $C(\omega) - \omega$ domains. Here the phase velocity is $C(\omega) = \omega/k(\omega)$ and $\kappa(\omega)$ is the skeletonized data (Schuster, 2015).

by (Groos et al., 2014). They concluded that the estimation of a priori quality factors is critical for inverting seismic waves in the near-surface zone. Pan et al. proposed to invert the Love-waves in the time domain to reconstruct the S-wave velocity model at the near surface (Pan et al., 2016).

To avoid the assumption of a layered medium and also mitigate FWI's sensitivity to local minima, we present a skeletonized inversion method that inverts the dispersion curves of surface waves for 2D or 3D velocity models (Li and Schuster, 2016). The picked dispersion curves are skeletonized data (Luo and Schuster, 1991b) that tend to make the objective function simpler, and hence this new method, denoted as wave equation dispersion inversion (WD), enjoys better convergence properties than FWI. This is similar to wave equation traveltime inversion (Luo and Schuster, 1991a), except picked dispersion curves rather than picked traveltimes are the input data.

The WD procedure is more robust than FWI because it replaces complicated surface-wave arrivals with simple dispersion curves in the wavenumber $k_x - \omega$ or phase-velocity $C(\omega) - \omega$ domains in Figure 1. The WD method presented in this paper is the adjoint-state method presented by (Zhang et al., 2015), who used a difference approximation to the gradient rather than an adjoint operation. Hence, our WD method is more than an order-of-magnitude faster for complicated models.

THEORY

The input data are z-component shot gathers excited by a vertical-component force at $\mathbf{s} = (x_s, 0)$ on the surface and recorded at $\mathbf{g} = (x_g, 0)$; and the skeletonized data consist of the picked dispersion curve $\kappa(\omega)_{obs}$ shown as the red dashed line in Figure 1. For a simplified exposition, we assume a single shot gather and the fundamental curve $\kappa(\omega)_{obs}$ associated with the Rayleigh waves, but WD is valid for any order or any number of dispersion curves. For higher-order dispersion wave, deeper S-velocity information can be inverted.

WD inversion

There are 4 steps in the WD method.

1. Skeletonized data. A shot gather is recorded in the $x-t$ domain and is Fourier transformed in time to give $D(\mathbf{g}, \omega)_{obs}$ for the shot at $(x_s, 0)$ and geophone at $(x_g, 0)$. A spatial Fourier transform in the x_g variable is then applied to $D(\mathbf{g}, \omega)_{obs}$ to give the spectrum $\tilde{D}(k, \omega)_{obs}$ in the (k, ω) domain, of which the dispersion curve $\kappa(\omega)_{obs}$ is picked for the fundamental mode. The dependency of $D(\mathbf{g}, \omega)_{obs}$, $\tilde{D}(k, \omega)_{obs}$, and $\kappa(\omega)_{obs}$ on the shot position \mathbf{s} is silent. A finite-difference method is used to solve the elastic wave equation for a specified starting model to get the predicted spectrum $\tilde{D}(k, \omega)$. The goal is to find the S-velocity model that predicts the picked dispersion curve $\kappa(\omega)_{obs}$.

2. Objective function. The dispersion misfit function ε is defined as the sum of squared dispersion residuals:

$$\varepsilon = \frac{1}{2} \sum_{\omega} \overbrace{(\kappa(\omega) - \kappa(\omega)_{obs})^2}^{residual = \Delta\kappa(\omega)}, \quad (1)$$

where $\kappa(\omega)$ is the predicted surface-wave wavenumber obtained by a 2D finite-difference solution to the elastic wave equation for a vertical point source at $(x_s, 0)$.

3. Gradient. A gradient optimization method is used to determine the S-slowness model $s(\mathbf{x})$ that minimizes ε , where the gradient is given by

$$\begin{aligned} \frac{\partial \varepsilon}{\partial s(\mathbf{x})} &= \sum_{\omega} \text{Re} \left[\frac{\partial \tilde{D}(\kappa(\omega)_{obs}, \omega)}{\partial s(\mathbf{x})} \tilde{D}(\kappa(\omega)_{obs}, \omega)^* \right], \\ &= \frac{1}{2\pi} \sum_{\omega} \text{Re} \left[\int \frac{\partial D(x_g, \omega)}{\partial s(\mathbf{x})} e^{ik(\omega)_{obs}x_g} dx_g \tilde{D}(\kappa(\omega)_{obs}, \omega)^* \right], \end{aligned} \quad (2)$$

The Fréchet derivative $\frac{\partial D(x_g, \omega)}{\partial s(\mathbf{x})}$ can be expressed as the Born approximation

$$\frac{\partial D(x_g, \omega)}{\partial s(\mathbf{x})} = -2s(\mathbf{x})W(\omega)G(\mathbf{g}|\mathbf{x})G(\mathbf{x}|\mathbf{s}), \quad (3)$$

where $W(\omega)$ is the source-wavelet spectrum and $G(\mathbf{g}|\mathbf{x})$ is the harmonic solution to the elastic wave equation for a vertical force at the point \mathbf{x} and a vertical-component particle-velocity recording at \mathbf{g} . This Green's function is for the mode of the fundamental Rayleigh wave.

Substituting equation 3 into equation 2 gives

$$\begin{aligned} \frac{\partial \varepsilon}{\partial s(\mathbf{x})} &= \frac{-s(\mathbf{x})}{\pi} \text{Re} \left[\sum_{\omega} \overbrace{W(\omega)G(\mathbf{x}|\mathbf{s})}^{source} \right. \\ &\quad \left. \overbrace{\left(\int G(\mathbf{g}|\mathbf{x})^* \{ e^{-ix_g \kappa(\omega)_{obs}} \tilde{D}(\kappa(\omega)_{obs}, \omega) \} dx_g \right)^* \right], \end{aligned} \quad (4)$$

where the source field is $f(\mathbf{x}, t) = \int e^{-i\omega t} G(\mathbf{x}|\mathbf{s})W(\omega)d\omega$ and the backpropagated data are $b(\mathbf{x}, t) = \int G(\mathbf{g}|\mathbf{x})^* \tilde{D}(\kappa(\omega)_{obs}, \omega) e^{-i(\omega t + x_g \kappa(\omega)_{obs})} d\omega$. This is the usual migration formula which

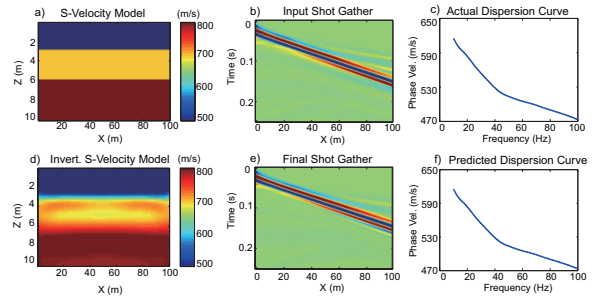


Figure 2: a) S-velocity model, b) a shot gather, and c) actual dispersion curve picked from the spectrum of the CSG. Lower row of images are the same except they are reconstructed after 20 iterations of the WD method.

says that the migration image at \mathbf{x} is formed by the zero-time lag of the backpropagated data $b(\mathbf{x}, t)$ correlated with the source field $f(\mathbf{x}, t)$. In practice, a preconditioned+regularized conjugate gradient or quasi-Newton method is used instead of the steepest descent method.

4. Conjugate gradient method, The optimal shear-slowness model $s(\mathbf{x})$ is obtained using the iterative conjugate gradient formula:

$$s(\mathbf{x})^{(k+1)} = s(\mathbf{x})^{(k)} - \alpha \frac{\partial \varepsilon}{\partial s(\mathbf{x})}, \quad (5)$$

where α is the step length, the gradient is defined in equation 4, the background S-slowness model is updated after each iteration, and the superscript denotes the k^{th} iteration. If there is more than one shot gather then there is an extra summation over shots with the understanding that $\kappa(\omega)_{obs}$ and $\tilde{D}(\kappa(\omega)_{obs}, \omega)$ have a silent dependence on the shot location.

NUMERICAL AND FIELD DATA TESTS

A weighted conjugate gradient method is used to test the WD method with elastic synthetic data and field data recorded over known fault structures. The constraint $V_p = \sqrt{3}V_s$ is used for all the models and density is constrained to be $\rho = 1000g/cm^3$.

Simple Three-Layer Model

A three-layer model is shown in Figure 2a where the S-velocity increases with depth. For input data, 20 vertical component shot gathers (see Figure 2b) are computed by solving the 2D elastic wave equation with 50 geophones located every 2 m on the surface. The dominant frequency of the source wavelet is 30 Hz with useful frequencies between 10 Hz and 80 Hz. The starting model for WD is the 1D model described by the blue dashed line in Figure 3c.

The dispersion curves are estimated using the procedure described in the previous section. The fundamental dispersion curve is picked for each shot gather in the $k-\omega$ domain and inverted by the WD method using an iterative conjugate gradient solver. After 20 iterations, the reconstructed model is shown in Figure 2d, where the predicted shot gather and dispersion

WD inversion

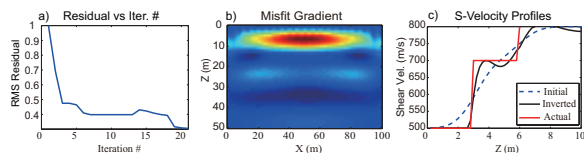


Figure 3: Plots of a) residual vs iteration number, b) misfit gradient for all of the shot gathers, and c) S-velocity profiles at $X = 50$ m.

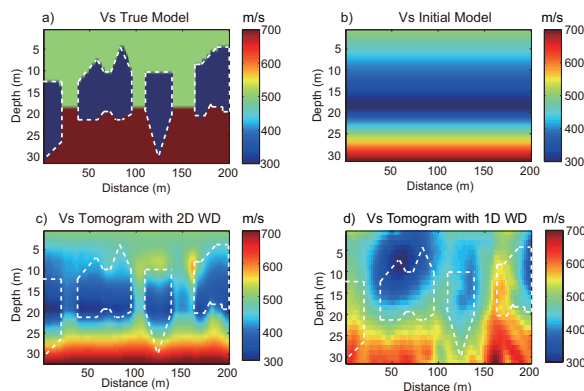


Figure 4: S-velocity 2D wave equation dispersion inversion. a) Vs true model; b) initial model; c) 2D WD tomogram after 15 iterations; d) 1D tomogram.

curve in e) and f) closely match the true values illustrated in b) and c), respectively.

The normalized RMS residual plotted against iteration number shows rapid convergence in Figure 3a, and the misfit gradient for all of the shot gathers in Figure 3b suggests that the shallow velocities down to about 3-6 m are accurately reconstructed. This is consistent with Figure 3c, where the reconstructed S-velocity profile (blue curve) over the center of the model is a good approximation to the actual velocity profile (red curve).

Low-Velocity Mineral Model

The objective of this synthetic test is to determine how well WD can detect the blue low-velocity anomalies in Figure 4a. These anomalies are based on realistic mineral deposits seen in an open-pit mine.

The input data are computed by solving the 2D elastic wave equation for 100 shot gathers, with the shots evenly distributed on the surface for a 10 Hz Ricker wavelet. Each shot is recorded by 100 receivers spaced at the same interval as the receivers. To convert the frequency variable to depth, we multiply the average S-velocity by $1/3$ and divide by the frequency. The phase velocity is computed as a function of frequency for each shot gather, frequency is converted to depth, and the $v_s(z)$ profile is generated at each shot position. The ensemble of 1D profiles are displayed as the S-velocity tomogram in Figure 4d. There is a rough but imprecise correspondence between the tomogram and the actual model in Figure 4a.

To generate a more accurate tomogram, the 2D WD method is

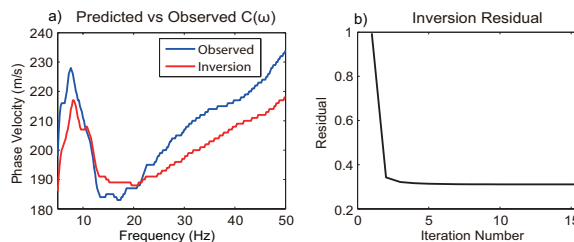


Figure 5: a) $C(\omega)$ for predicted (red) and observed dispersion (blue) curves for a CSG and b) dispersion misfit residuals plotted against iteration number.

used to invert the data. In this case, only 25 shot gathers are employed with a 8 m shot interval. Figure 4b is the initial gradient model, and the fundamental dispersion curve is picked for each shot gather and inverted by the WD method. After 15 iterations, the reconstructed model is shown in Figure 4c. This tomogram shows much better correspondence to the actual model than does the 1D tomogram. The predicted and observed dispersion curves are plotted against iteration number in Figure 5. After 15 iterations, the normalized misfit residual decreased to 0.3 and shows an acceptable fit to the data.

Qadimah Fault Controlled Noise Source Seismic Data

A controlled noise source (CNS) seismic survey is conducted across the Qadimah fault, a normal fault near the KAUST campus. The geophone line consists of 60 receivers at a 10 m spacing and a noise-making truck is driven around the survey line for 2 hours. The resulting seismic noise is recorded at each of the traces. Then, the traces are broken up into small windows, and each window of arrivals is correlated with the corresponding window of arrivals in other traces to give a virtual CSG (Hanafy et al., 2015). Stacking the virtual CSGs for the same source position gives the virtual shot gather.

A common offset gather (COG) is shown in Figure 6a with the source-receiver offset of 50 m. The dashed lines in Figure 6a indicate the location of the Qadimah fault, which is consistent with the lateral velocity decrease in the P-velocity tomogram in Figure 6b. The P-velocity tomogram is computed by inverting the first-arrival traveltimes. The shot gather is transformed into the f - v domain by a Radon transform and the maximum energy values of the dispersion curve are picked. Figure 6c shows the S-velocity tomogram obtained from the traditional 1D inversion of dispersion curves. The tomogram roughly estimates the position of the Qadimah fault according to the low S-wave velocity structure. Then, the 2D WD method is applied to the picked dispersion curves to give the S-velocity tomogram in Figure 6d, where there is a low-velocity zone on the downthrown side of the fault. This is consistent with the P-velocity tomogram in Figure 6b and the COG profile in Figure 6a for 150 m $< x < 300$ m. As the surface waves enter the fault zone there is strong dispersion in the surface-wave arrivals.

It is difficult to assess the accuracy of the 2D WD tomogram, but it appears to have much more complexity than the simpler 1D tomogram in Figure 6c. In fact, the 1D tomogram appears

WD inversion

to be too simple to fully explain the the complexity of events in the Figure 6a COG.

SUMMARY

We present the theory for wave equation inversion of dispersion curves, where the dispersion misfit function is the difference between the wave-numbers along the predicted and observed dispersion curves. The S-wave velocity model is updated by migrating the weighted data, where the weight is proportional to the dispersion residual. It largely overcomes the expense of finding the Fréchet derivative by a finite-difference approximation. Numerical simulations suggest that WD inversion is effective for selected 2D velocity models where the dispersion curves can be readily identified. The corresponding 2D tomograms are more accurate than the ones inverted by assuming a local 1D velocity model over each common shot gather. Tests on both synthetic and field data suggest that reasonable velocity models can be inverted to reveal the presence of faults.

ACKNOWLEDGMENTS

We thank the 2016 sponsors of Center for Subsurface Imaging and Fluid Modeling (CSIM) at King Abdullah University of Science and Technology (KAUST) for their support. We also send the appreciation to KAUST Supercomputing Laboratory.

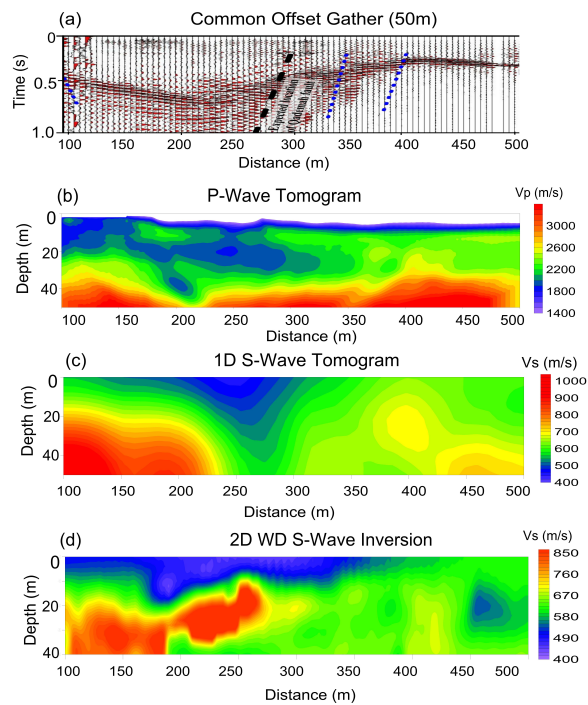


Figure 6: Results from Qademah data for a) common offset gather, b) P-velocity tomogram inverted from 1st-arrival traveltimes, c) S-velocity tomogram inverted by the standard 1D inversion of dispersion curves, and d) S-velocity tomogram computed by 2D WD inversion of dispersion curves.

EDITED REFERENCES

Note: This reference list is a copyedited version of the reference list submitted by the author. Reference lists for the 2016 SEG Technical Program Expanded Abstracts have been copyedited so that references provided with the online metadata for each paper will achieve a high degree of linking to cited sources that appear on the Web.

REFERENCES

- Bergamo, P., D. Boiero, and L. V. Socco, 2012, Retrieving 2D structures from surface-wave data by means of space-varying spatial windowing: *Geophysics*, **77**, no. 4, EN39–EN51, <http://dx.doi.org/10.1190/geo2012-0031.1>.
- Brossier, R., J. Virieux, and S. Operto, 2008, Parsimonious finite-volume frequency-domain method for 2-D P–SV-wave modelling: *Geophysical Journal International*, **175**, 541–559, <http://dx.doi.org/10.1111/j.1365-246X.2008.03839.x>.
- Dou, S., and J. B. Ajo-Franklin, 2014, Full-wavefield inversion of surface waves for mapping embedded low-velocity zones in permafrost: *Geophysics*, **79**, no. 6, EN107–EN124, <http://dx.doi.org/10.1190/geo2013-0427.1>.
- Evison, F. F., C. E. Ingham, and R. H. Orr, 1959, Thickness of the earth's crust in Antarctica: *Nature*, **183**, 306–308, <http://dx.doi.org/10.1038/183306a0>.
- Groos, L., M. Schäfer, T. Forbriger, and T. Bohlen, 2014, The role of attenuation in 2D full-waveform inversion of shallow-seismic body and Rayleigh waves: *Geophysics*, **79**, no. 6, R247–R261, <http://dx.doi.org/10.1190/geo2013-0462.1>.
- Hanafy, S. M., A. AlTheyab, and G. T. Schuster, 2015, Controlled noise seismology: 85th Annual International Meeting, SEG, Expanded Abstracts, 5102–5106, <http://dx.doi.org/10.1190/segam2015-5906063.1>.
- Luo, Y., and G. T. Schuster, 1991a, Wave equation inversion of skeletalized geophysical data: *Geophysical Journal International*, **105**, 289–294, <http://dx.doi.org/10.1111/j.1365-246X.1991.tb06713.x>.
- Luo, Y., and G. T. Schuster, 1991b, Wave-equation travelt ime inversion: *Geophysics*, **56**, 645–653, <http://dx.doi.org/10.1190/1.1443081>.
- Pan, Y., J. Xia, Y. Xu, L. Gao, and Z. Xu, 2016, Love-wave waveform inversion in time domain for shallow shear-wave velocity: *Geophysics*, **81**, no. 1, R1–R14, <http://dx.doi.org/10.1190/geo2014-0225.1>.
- Park, C. B., R. D. Miller, J. Xia, 1998, Imaging dispersion curves of surface waves on multi-channel record: 68th Annual International Meeting, SEG Expanded Abstracts, 1377–1380, <http://dx.doi.org/10.1190/1.1820161>.
- Romdhane, A., G. Grandjean, R. Brossier, F. Rejiba, S. Operto, and J. Virieux, 2011, Shallow-structure characterization by 2d elastic full-waveform inversion: *Geophysics*, **76**, no. 3, R81–R93, <http://dx.doi.org/10.1190/1.3569798>.
- Schuster, G., 2015, Seismic inversion: SEG.
- Sears, T. J., S. Singh, and P. Barton, 2008, Elastic full waveform inversion of multi-component OBC seismic data: *Geophysical Prospecting*, **56**, 843–862, <http://dx.doi.org/10.1111/j.1365-2478.2008.00692.x>.
- Sheng, J., A. Leeds, M. Buddensiek, and G. T. Schuster, 2006, Early arrival waveform tomography on near-surface refraction data: *Geophysics*, **71**, no. 4, U47–U57, <http://dx.doi.org/10.1190/1.2210969>.
- Socco, L., P. Bergamo, and F. Garofalo, 2014, Surface wave dispersion analysis — From local 1D models to tomography: Presented at the 76th EAGE Conference and Exhibition — Workshops, <http://dx.doi.org/10.3997/2214-4609.20140528>.

- Solano, C. P., D. Donno, and H. Chauris, 2014, Alternative waveform inversion for surface wave analysis in 2-D media: *Geophysical Journal International*, **198**, 1359–1372, <http://dx.doi.org/10.1093/gji/ggu211>.
- Tarantola, A., 1984, Inversion of seismic reflection data in the acoustic approximation: *Geophysics*, **49**, 1259–1266, <http://dx.doi.org/10.1190/1.1441754>.
- Tian, G., D. W. Steeples, J. Xia, and K. T. Spikes, 2003, Useful resorting in surface-wave method with the autojuggie: *Geophysics*, **68**, 1906–1908, <http://dx.doi.org/10.1190/1.1635043>.
- Xia, J., R. D. Miller, C. B. Park, J. Ivanov, G. Tian, and C. Chen, 2004, Utilization of high-frequency Rayleigh waves in near-surface geophysics: *The Leading Edge*, **23**, 753–759, <http://dx.doi.org/10.1190/1.1786895>.
- Yuan, Y. O., F. J. Simons, and E. Bozdağ, 2015, Multiscale adjoint waveform tomography for surface and body waves: *Geophysics*, **80**, no. 5, R281–R302, <http://dx.doi.org/10.1190/geo2014-0461.1>.
- Zhang, Z., Y. Liu, and G. Schuster, 2015, Wave equation inversion of skeletonized surface waves: 85th Annual International Meeting, SEG, Expanded Abstracts, 2391–2395, <http://dx.doi.org/10.1190/segam2015-5805253.1>.